DYNAMIC BEHAVIOR SIMULATIONS OF PULVERIZED BIOMASS RDF COMBUSTION

JAI-HOUNG LEU
GENERAL EDUCATION CENTER
YU-DA UNIVERSITY, 36143, R.O.C. TAIWAN
E-MAIL: JAHONLEU@YAHOO.COM.TW

ABSTRACT. This study used a CFD solver, CFX, to simulate the pulverized biomass refused-derived fuel (RDF) dynamic combustion behavior inside a wall-fired furnace, and investigated the effects of combustor geometry, pulverized biomass RDF traces, and burner positions on its performance under various operating conditions. The results showed that the interactions between various burners can affect the pulverized biomass RDF dynamic behavior significantly. In particular, the probability of pulverized biomass RDF hitting the wall is controlled by the down-fired rate as well as inlet conditions. Finally, the NOx concentrations inside the furnace are predicted in the optimal operating condition (Case 3). The results can be used as a design reference for the optimal operational combustion condition of pulverized biomass RDF.

AMS Classification: 37M05, 76F20, 76F25
Keywords: Pulverized RDF, Swirl flow, Recirculation zone.

1. INTRODUCTION

The air used for combustion is drawn by fan and distributed into the four guide blades, and then entered into the four lances at nearly tangent angle to inject mixed fuel for the central axis fuel (pulverized biomass RDF). In other words, four burners are used to stabilize flame and increase combustion efficiency.

JOURNAL OF DYNAMICAL SYSTEMS & GEOMETRIC THEORIES
VOL. 9, NUMBER 1 (2011) 11-25.

The flow-field simulation by CFX was detailed in [3]. It is discussed the prediction accuracy of CFX, and found that CFX has high prediction accuracy thoroughly. In addition, the flow-field of four burners is present. One high limit ratio and four burners flow field are taken as the display flow field.

This study used CFX software to simulate dynamic behavior of pulverized biomass RDF combustion in furnace. The results can be used as a reference for the optimal design of burner and furnace to increase energy combustion efficiency and reduce pollution emission with pulverized biomass RDF combustion.

2. Research Method

Numerical model and method in this study were discussed in this section.

2.1. Governing Equations. This paper utilizes 3-dimensional Cartesian coordinates. The turbulent model uses standard K–ε model to simulate turbulent stress terms and turbulent viscosity coefficient. The side-wall functions are adopted for treatment of near-wall flow-field to reduce computer calculation time and memory capacity. Continuity equation, momentum equations, and energy equation are expressed by the general equations:

$$\frac{\partial}{\partial t}(\rho\phi) + \nabla.(\rho U\phi) - \nabla.(\Gamma_\phi \nabla_\phi) = S_\phi.$$

Where $\frac{\partial}{\partial t}(\rho\phi)$ is the transient term, div $(\rho U\phi)$ is the convection term, div $(\Gamma_\phi \nabla_\phi)$ is the diffusion term, S_ϕ is the source term for the variable ϕ.

2.2 Combustion model. Smoot and Pratt [4] divided the components of coal particles are moisture, raw coal, char and ash. When simulating the pulverized coal combustion process, the reaction pattern is divided into de-volatilization and char oxidation.

De-volatilization is the second reaction pattern proposed by Ubhayakar (1976) [5]. It is assumed that de-volatilization reaction pattern experiences twice reaction. In the first reaction, lower particle temperature and lower volatilization *Y1* is provided. In the second reaction, higher particle temperature and higher volatilization *Y2*, *K1*, *K2* which are reaction constants are supplied.

Since de-volatilization of char particles is slow, the method proposed by Field [1] and Gibb [2] is adopted in this study. The coal particles are considered as spherical particles. The periphery is surrounded by the stagnant boundary layer, and the oxygen can react with char particles by diffusing through the boundary layer. When oxygen diffuses into the char particle inner holes, it oxidation reaction with char particles occurs. The pulverized biomass RDF is simulated by using Lagrangian method.

NOx pollutants are emitted from combustion of pulverized biomass RDF. The *NOx* Model is a simplified reaction model. Three rapid reaction mechanisms are applied in the pulverized biomass RDF combustion to predict formation of *NOx*: a) HCN reaction mechanism; b) *NO* formation reaction mechanism, c) *NO* consumption reaction (reduction reaction *NO* and *HCN*). In addition, the simulated pollutants are small, and thus, the impact on environmental density and specific heat is neglected.

2.3. Inlet conditions. The wall-fired furnace in this study has premix burners that are comprised of four pulverized biomass RDF lances. This paper simulates the dynamic behavior of wall-fired furnace under different operating conditions and discusses impact of operating parameter variation on flow-field. The four cases are as follows:

	pulverized biomass RDF supply rate	Air carrying velocity	Swirled air velocity	pulverized biomass RDF size
Case 1	2.3565 kg/s	9.04 m/s	35 m/s	48μm
Case 2	4.7130 kg/s	9.04 m/s	35 m/s	48μm
Case 3	1.7498 kg/s	8 m/s	35 m/s	48μm
Case 4	1.7498 kg/s	8 m/s	35 m/s	12μm

In each case, swirl angle of each burner is 45?, and the number of traced pulverized biomass RDF is 16, and accordingly 64 pulverized biomass RDF traces were tracked.

The assumed pulverized biomass RDF components are as follows:

Volatile (%)	Fixed Carbon (%)	Ash(%)	Moisture(%)
22.0	70.0	3.0	5.0

2.4. Outlet condition. The outlet conditions are assumed to be the total development conditions, i.e. $\frac{\partial \phi}{\partial z} = 0$, ϕ represents relevant variables of u, v, w, k, ε, h, f, g.

2.5. Wall condition. Assumed wall has no slip condition, and adiabatic.

3. Results and Discussions

It is discussed that the CFX accuracy rate of pulverized coal flow-field and the 3-dimensional combustion flow-field with large velocity difference in reference [6]. Although, the flame holder is different, the flame stability of back flow regions and flow-field was similar in this study. Comparison of results of isothermal and two-phase flow fields proves that CFX has good reliability.

The wall-fired furnace in this study has premix burners that are comprised of four pulverized biomass RDF lances and contained four inlets. Therefore, boundary-fitted coordinates are used to reduce boundary condition errors. Swirl inlet of pulverized biomass RDF requires description of concentric grids, thus, the concentric grids totaled to 37500 (Figure 1).

The flow-field of the wall-fired furnace is simulated by using four groups of operating conditions for the discussion of the impacts of the conditions. Lastly, NOx concentration distribution of case 3 can be predicted. In each case, the swirl angle of each burner is 45?, and the number of traced pulverized biomass RDF is 16. Accordingly, 64 pulverized biomass RDF traces are tracked in total. Convergence criteria is the absolute value of mass source residue attains 10^2.

The interactions between various swirl burners form a clockwise swirl in the periphery and counterclockwise swirl in the inner due to rectangular boundary. Figures 2 show the back flow of dimension vector and z direction in Case 1. In Figure 2, near flow field (z=1.04), the center of four burners may form a counterclockwise swirl. However, the inlet of each burner causes swirl dissipation. The two burners in the figure have distortion and displacement of back flow regions due to the overall swirl direction. The top recirculation zone is formed by the upward distortion caused by strong upward side air injected from inlet of burners. Moreover, burner inlet results in re-attachment of jets, causing top back flow region. The back flow is more obvious in the lower stream (z=2.08 to 3.12). Based on the temperature distribution, the temperature in the recirculation zone is too low, without flame stabilization effect. The lower recirculation zone is formed by (partial) jets due to lower cavitations. Jets bend upwards due to boundary and buoyancy effects, as shown in the figure. Moreover, the inner recesses of the furnace made the back pressure of jets obvious. As seen, the flame stabilization effect remains in the bottom combustion inlets, and may have positive impact on the combustion rate in the furnace cavity. Figure 3 shows the contour map of the recirculation zone at velocity vector and in w direction under different y sections. The flow of fluid body in the furnace cavity is very complex. In the exchange zone of high kinetic energy, when y=3.0, there are some swirls under the y section. With increase of height, the swirls dissipate due to fast expansion of gas after combustion, and the vertical swirls finally disappear because of inlet positions. Finally, the vertical swirled flow disappears due to approaching the outlet position. In addition, the obvious swirled flow appears at y=6.54 that is the extension of the swirl red flow behind the # 4 burner.

Figure 4 shows the distribution of temperature above different sections. Near flow-field of the burners, four flames appeared. When z=1.04, edge flame is pulled upwards possibly because of entire clockwise movement. When z=2.08, the left top combustion reaction becomes weaker due to flame mechanism (see Figure 2). The situation is more obvious when z=3.12. In the downstream (z?4.16), the zone with lower temperature can be found in the right side. According to the velocity vector of the Figure 2, there is no notable swirl structure in downstream of Z plane. Sufficient energy exchange has caused lower temperature zones. Figure 5 shows the distribution of temperature above different X planes. The spacing between burners is large enough, and thus no flame is mixed. The right top burner's flame distortion is serious, and almost become vertical flame. The flame on the left top has slight upward distortion affected by inlet boundary. The top high temperature zone was formed by the second reaction due to re-attachment. The outlet temperature is uniform (see Figure 4), because capacity of furnace cavity is large enough.

Figure 6 shows the pulverized biomass RDF trace. As seen, pulverized biomass RDF form cone shape and rotationally spread due to swirled air after injecting into the furnace. In the four burners, the pulverized biomass RDF injected have 1/32 probability of hitting the wall, indicating that the wall surface may have slugging problem.

Figure 7 is the isothermal map of Case 2. At the same mass flow rate in the inlet, the injection rate of the pulverized biomass RDF is adjusted from 2.3565kg/s to 4.7140kg/s. That is, combustion load of the furnace cavity is increased. After comparison of flow-field structure and back flow region, the increase of combustion load only has slight impact, and thus temperature distribution structure inside the furnace is not obviously affected. The main difference is the increase of furnace cavity temperature. Moreover, the increase of flame temperature and weak mix structure of second flow on Y tangent planes cause the non-uniform outlet temperature distribution. As shown in Figure 7, the jet's second reaction of left top burner tends to be more obvious.

In Case 1, the inlet temperature is about 1200K. To prevent high inlet temperature, the injection rate of pulverized biomass RDF in Case 3 is 1.7498kg/s to reduce furnace cavity load. Figure 8 is the isothermal map of Case 3 under the different x tangent planes. As seen, the temperature of the furnace is lower than that in Case 1, and the outlet temperature is 1050K. The high temperature of second reaction above the left top burner is not obvious in Case 3, because the time of burnout shortens after reduction of furnace load. The high-temperature gas and lower-temperature air can be mixed evenly.

Case 3 and Case 4 have the same conditions. The pulverized biomass RDF size is adjusted from 48μm to 12μm, and the impact of pulverized biomass RDF size variation on flow-field structure and temperature distribution is discussed. After comparison of velocity vector on the different X tangent planes and recirculation zone distribution, pulverized biomass RDF size variation has no impact. The isothermal map under the different x tangent planes, as shown in Figure 9 is compared with Figure 8. The distribution tendency of the temperature field has no change. However, in Case 4, high temperature occurs early due to smaller pulverized biomass RDF size. Figure 10 shows the comparison of pulverized biomass RDF traces. As seen, the probability of pulverized biomass RDF hitting the wall in Case 4 is smaller than that of Case 3, because the pulverized biomass RDF size of Case 3 is larger, with greater initial momentum. As a result, their movement trace is not affected by the fluid body, and it is easier for pulverized biomass RDF to hit the wall. In case 3 and case 4, the difference between pulverized biomass RDF sizes. i.e. 48μm and 12μm, is not significant. Therefore, the pulverized biomass RDF size has no significant impact on dynamic behavior of the furnace. Figure 11 shows the NO concentration distribution of Case 3 under different x tangent planes. As seen, NO concentration is related to high temperature zone.

4. Conclusions

This study used CFX to simulate the dynamic behavior of pulverized biomass RDF combustion in wall-fired swirl furnace, and discussed the relationship between velocity of flow-field in the furnace and temperature under different loading conditions. The results showed that, high temperature zone was formed in the upper walls of the four burners at the same injection rate. This was obvious with increase of F/A. If reducing injection rate of the top burners, the top high temperature zone could be improved, but uniformity of inlet temperature became worse. Under the same inlet condition, the change of the pulverized biomass RDF size could reduce probability of pulverized biomass RDF hitting the wall and the related slugging effects, but, not obvious. The optimal operational condition for pulverized biomass RDF combustion in furnace is concluded that the supply rate is 1.7498 kg/s and the size is 48 μm in addition to the air carrying velocity is 8 m/s and the swirled air velocity is 35 m/s.

References

[1] Field, M.A., gill, B.B., and Hawksley, P.G.W., "The combustion of Pulverized Coal, "British coal Utilization Research Association, Leatherhead, Surrey, 175-187 (1967).

[2] Gibb, J. "Combustion of residual char Remaining after De-volatilization, Lecture at course of Pulverized Coal Combustion," Mechanical engineering Dept, Imperial College, London (1985).

[3] Li, C.H., Chi, C.C., "Effect of combustor geometry on combustion characteristics", the 16^{th} Symposium (International) on combustion, the Combustion Association of R.O.C, 125-132 (1991).

[4] Smoot, L.D., and Pratt, D.T. (eds), Pulverized Coal combustion and gasification, Plenum Press, New York (1979).

[5] Ubhayakar, S.J., Stickler, D.B., Von Rosenburg, C.W. and Gannon, R. E., "Rapid Devolatilization of Pulverized Coal in Hot combustion Gases, the 6^{th} Symposium (International) on combustion, the combustion Association of R.O.C., 426-438 (1976).

[6] Zhou, L.X., Lin, W.Y., Luo, W.W. and Huang X.Q., "Gas-Particle Flow and Coal Combustion in a burner/combustor with High-Velocity Jets" Combustion and Flame., 125-138 (1994).

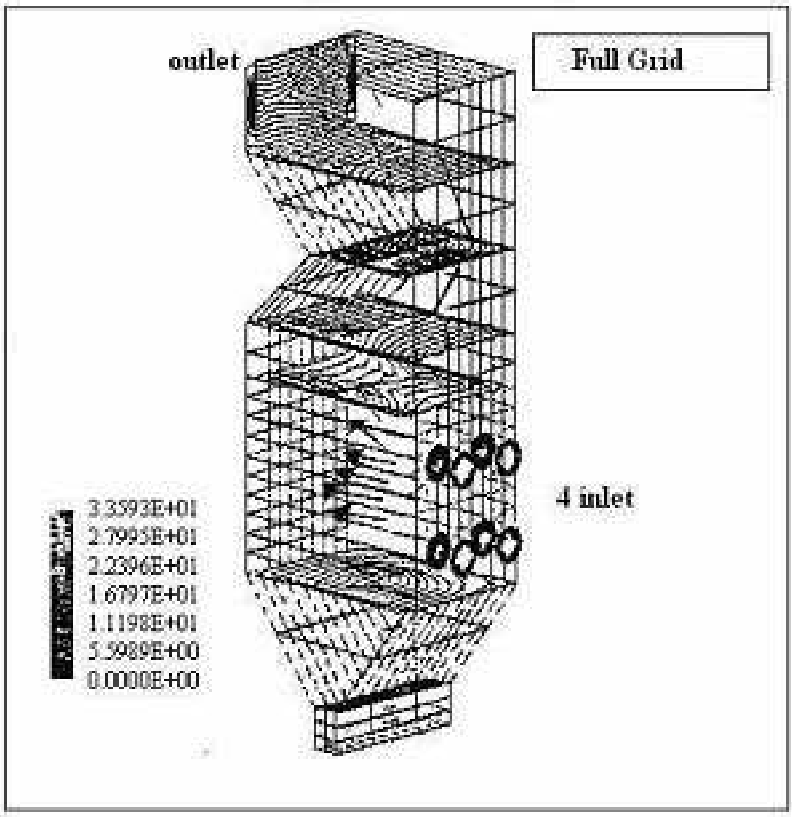

Figure 1 Distribution grate points of wall-fired furnace

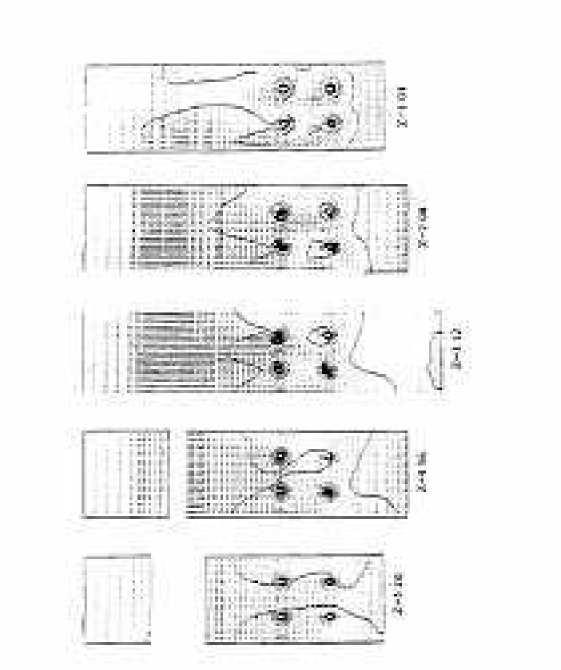

Figure 2 Contour map of velocity vector and w=0 of Case 1 under different z tangent planes

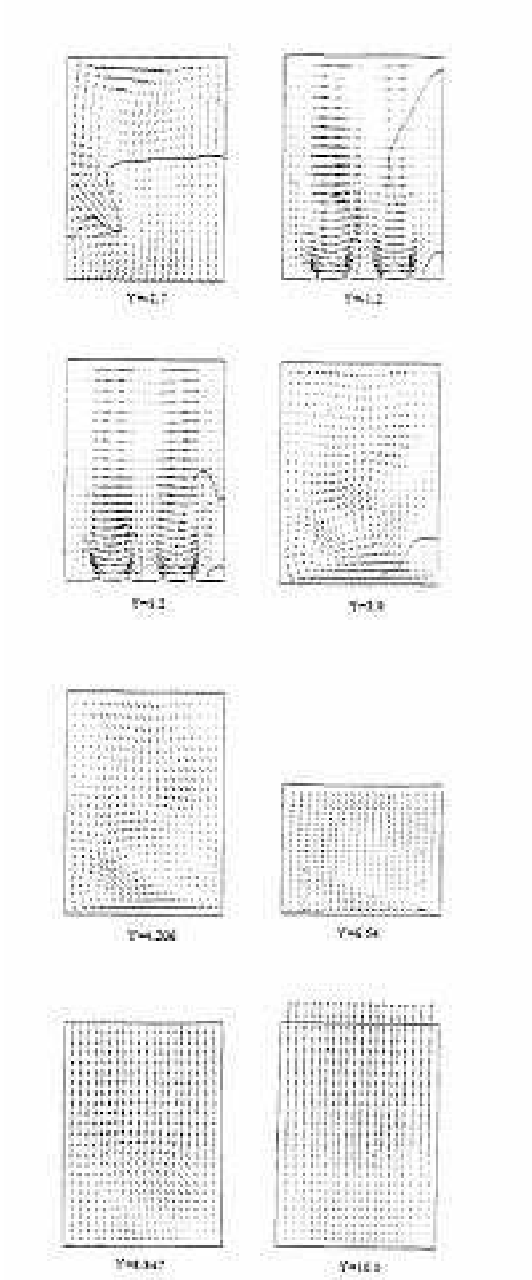

Figure 3 Contour map of velocity vector and w=0 of Case 1 under different y tangent planes

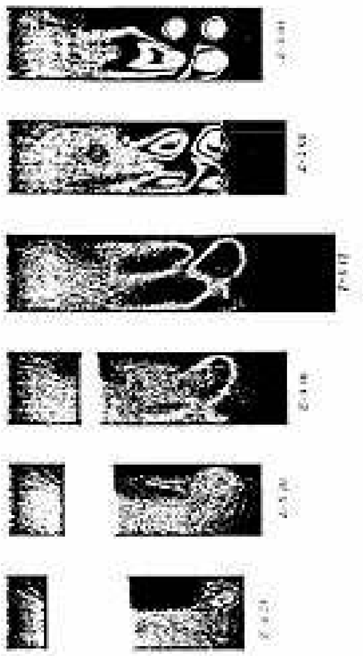

Figure 4 Temperature distribution of Case 2 under different z tangent planes

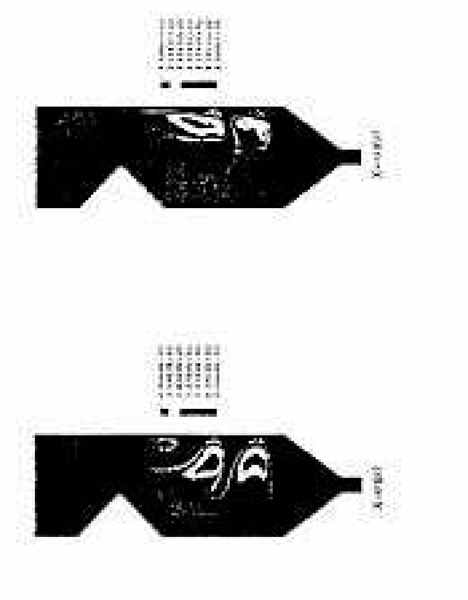

Figure 5 Temperature distribution of flow-field of Case 1 under different x tangent planes

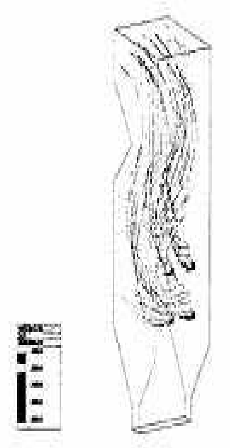

Figure 6 Pulverized biomass RDF particle trace of Case 1

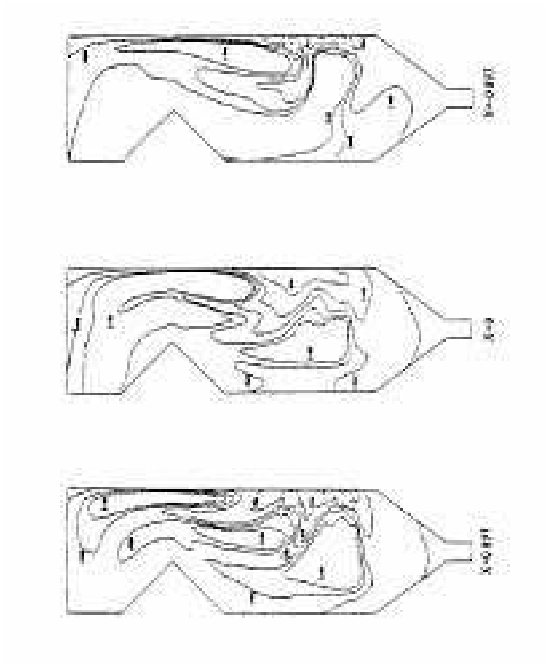

Figure 7 Isothermal chart of flow-field of Case 2 under different x tangent planes

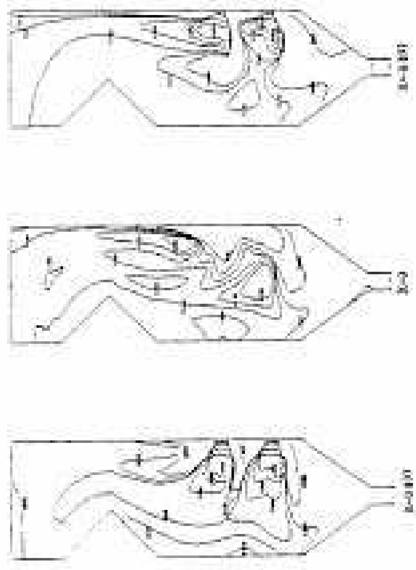

Figure 8 Isothermal chart of flow-field of Case 3 under different x tangent planes

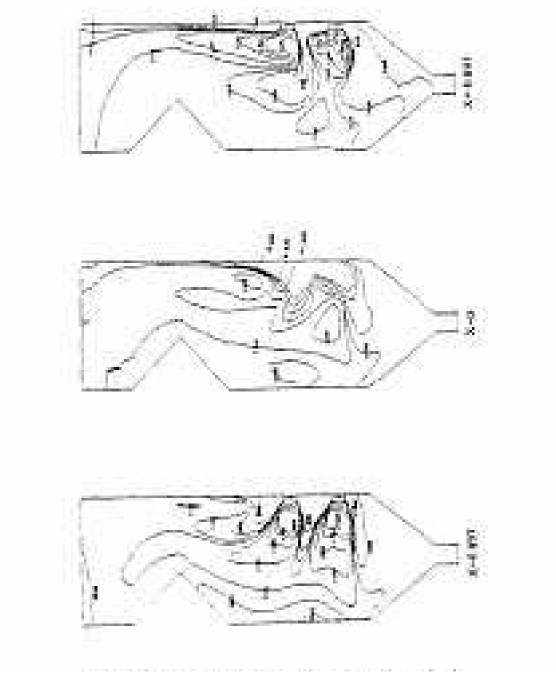

Figure 9 Isothermal chart of flow-field of Case 4 under different x tangent planes

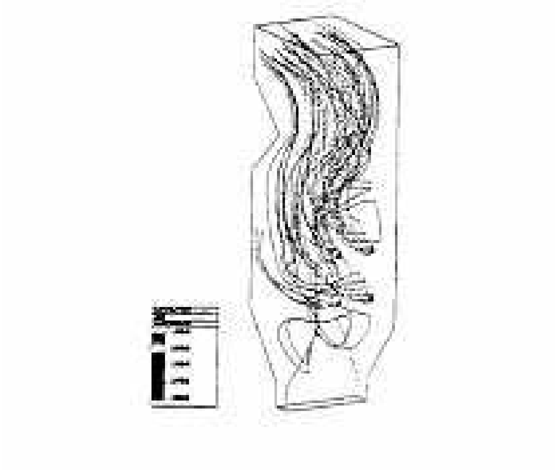

Figure 10 Pulverized biomass RDF particle trace of Case 4

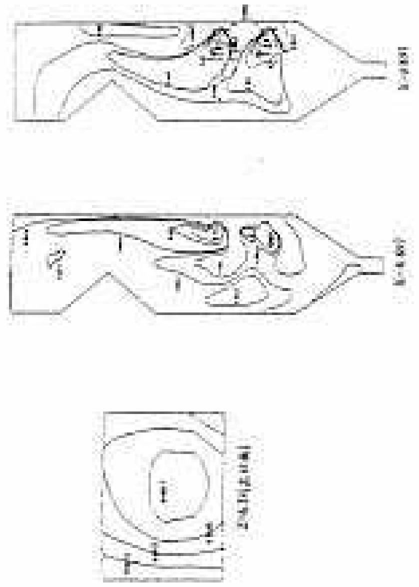

Figure 11 No mass fraction distribution of Case 3 under different tangent planes